Chaos in two-loop negative feedback systems

J. C. Bastos de Figueiredo,[1] L. Diambra,[2] Leon Glass,[3] and C. P. Malta[4]

[1]*Instituto do Coração, Universidade de São Paulo, Avenida Dr. Eneas de Carvalho Aguiar, 44, 05403-000 São Paulo, São Paulo, Brazil*
[2]*Instituto de Ciências Biomédicas, Universidade de São Paulo, Avenida Lineu Prestes, 1524 ICB1, 05508-900 São Paulo, São Paulo, Brazil*
[3]*Department of Physiology, McGill University, 3655 Drummond Street, Montreal, Quebec, Canada H3G 1Y6*
[4]*Instituto de Física, Universidade de São Paulo, Caixa Postal 66318, 05315-970 São Paulo, São Paulo, Brazil*

Multiloop delayed negative feedback systems, with each feedback loop having its own characteristic time lag (delay), are used to describe a great variety of systems: optical systems, neural networks, physiological control systems, etc. Previous investigations have shown that if the number of delayed feedback loops is greater than two, the system can exhibit complex dynamics and chaos, but in the case of two delayed loops only periodic solutions were found. Here we show that a period-doubling cascade and chaotic dynamics are also found in systems with two coupled delayed negative feedback loops.

I. INTRODUCTION

A variety of oscillatory phenomena are observed in biology with well known examples in neurology, cardiology, hematology, and ecology. A fundamental characteristic of these dynamical systems is that their behavior depend on time delays [1–5]. Time delays arise as a consequence of intrinsic biological and physical processes such as reproduction of cells and organisms, conduction of excitation, and diffusion of chemical signals. For instance, control in physiological systems is accomplished by multiple negative feedback loops that are, in general, delayed. A basic question is whether the fluctuating dynamics observed in physiological and other biological systems are due to the instabilities in the basic control systems, or may be due to other factors such as a fluctuating and noisy environment.

It is well known that a single-loop negative feedback system with a time delay can display stable limit cycle oscillations, but it does not exhibit chaos [5–8] due to the monotonicity of the feedback function. A single-loop system will exhibit chaotic dynamic only if it has mixed (the corresponding function has an extremum) feedback [2,8–12]. Most physiological control systems have multiple negative feedback loops (heart rate [13–15], blood pressure [16,17], motor activity [18–22]), and the dynamics result from the interplay of the various feedback controls. Although it would appear that multiple delayed feedback loops could provide benefits to the organism, with some feedbacks operating quickly (short delay) and others slowly (longer delay), mathematical properties of systems with multiple delays are not well understood. Somewhat in opposition to the view that multiple delayed feedback loops are more stable than single loops [4,20], it has been shown that multilooped delayed negative feedback systems may exhibit complex dynamics, including period-doubling bifurcations leading to chaos, if the number of delayed negative feedback loops is greater than two [18,23]. However, the conditions needed for chaos are not known, and chaos has not been found to date in systems with two negative feedback delayed loops [18,23].

The mathematical analysis of multiple-delay differential equations has to be restricted to special cases due to the high dimensionality of the problem. The linear stability of systems with two time delays has been studied by several authors [24–29], but there is not a complete analysis since different authors consider different subsets of the parameter space. As parameters are varied, one usually observes a Hopf bifurcation leading to oscillations. The current work was undertaken to search for chaotic dynamics in a system with two delayed negative feedback loops. A nonlinear model with N delayed negative feedback loops is presented in Sec. II. In Sec. III we present a linear stability analysis for $N=2$, and in Sec. IV we demonstrate bifurcations and chaotic dynamics in a system with two delayed negative feedback loops. We discuss the results in Sec. V.

II. THE MODEL

We consider a system of N delayed feedback loops described by the following equations:

$$\dot{x}_i = F_i(P_{\tau_i}) - x_i, \quad i = 1, \ldots, N, \qquad (1)$$

where the subscript τ_i indicates the delayed time argument $(t - \tau_i)$, and

$$P = N^{-1} \sum_{i=1}^{N} x_i \qquad (2)$$

is the variable of primary interest controlled by N feedback loops. The feedback control of x_i takes place only by way of the variable P that we have assumed to be the average of x_i just for simplicity (we could have considered a weighted average with the weights being treated as parameters).

The functions $F_i(P_{\tau_i})$ are nonlinear functions depending on P at time $t - \tau_i$. Since we are interested in negative feedback, we assume that $F_i(X_{\tau_i})$ is a monotonically decreasing function,

$$F_i(P_{\tau_i}) = \frac{\theta_i^{n_i}}{\theta_i^{n_i} + P_{\tau_i}^{n_i}}, \quad 0 < \theta_i < 1, \tag{3}$$

where n_i and θ_i are parameters governing the steepness and threshold of the sigmoidal function F_i, respectively. For simplicity we shall consider $n_i = n$, $\forall i$ [18,23]. Under this assumption Eqs. (1) lead to the following multidelayed differential equation for $P(t)$ (2):

$$\dot{P}(t) = -P(t) + \frac{1}{N} \sum_{i=1}^{N} \frac{\theta_i^n}{\theta_i^n + P_{\tau_i}^n}. \tag{4}$$

The above Eq. (4) can also be used to describe one neuron having N self-inhibitory delayed loops, and constitutes a generalization of the equations used by Gopalsamy and Leung [30] to investigate the dynamical characteristics of a firing neuron.

It should be remarked that in the limit $n \to \infty$ the Eq. (4) becomes piecewise linear and can be readily integrated. This limit is very useful to check the numerics of the finite n case that requires numerical integration.

As already mentioned, Eq. (4) cannot exhibit chaos if $N = 1$ [5–8], and it has been found to exhibit complex dynamical behavior if $N \geq 3$ [23]. We are here interested in the case $N = 2$ for which only periodic or quasiperiodic dynamics have been found. In the following section we make the linear stability analysis of Eq. (4) in the case $N = 2$.

III. LINEAR STABILITY ANALYSIS

Setting $N = 2$ Eq. (4) becomes

$$\dot{P}(t) = -P(t) + \frac{1}{2} \sum_{i=1}^{2} \frac{\theta_i^n}{\theta_i^n + P_{\tau_i}^n}. \tag{5}$$

The steady-state $\tilde{P}$ is obtained as a solution of

$$\tilde{P} = \frac{1}{2} \sum_{i=1}^{2} \frac{\theta_i^n}{\theta_i^n + \tilde{P}^n}. \tag{6}$$

Introducing the variable

$$\delta P(t) = P(t) - \tilde{P}, \tag{7}$$

and keeping only the linear terms of the Taylor expansion of Eq. (5) we obtain the linear delay differential equation,

$$\frac{d}{dt} \delta P(t) = -\delta P(t) - \frac{1}{2} \sum_{i=1}^{2} g_i(\tilde{P}, n, \theta_i) \delta P_{\tau_i}, \tag{8}$$

where

$$g_i(\tilde{P}, n, \theta_i) = n(\tilde{P})^{n-1} \frac{\theta_i^n}{(\theta_i^n + \tilde{P}^n)^2}. \tag{9}$$
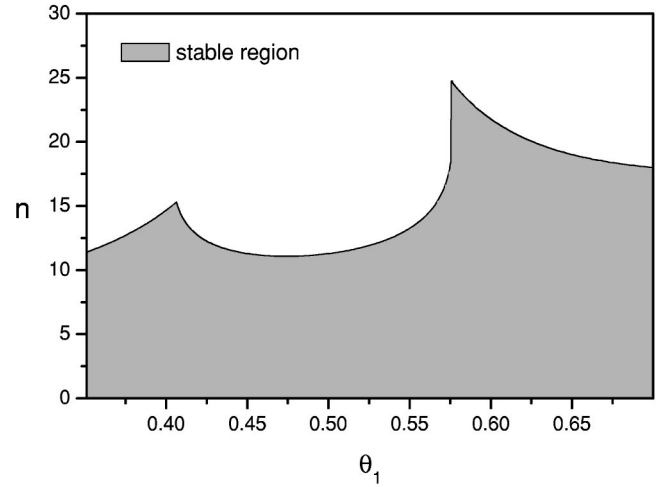
FIG. 1. Stability region in the plane (θ_1, n) for fixed parameters value $\tau_1 = 0.26, \tau_2 = 2.00, \theta_2 = 0.491$. The parameter θ_1 is in arbitrary units, and n is dimensionless.

The linear stability of the stationary state is then determined by the roots of the associated characteristic equation

$$\lambda + 1 = -\frac{1}{2} \sum_{i=1}^{2} g_i(\tilde{P}, n, \theta_i) \exp(-\lambda \tau_i). \tag{10}$$

The stationary state $\tilde{P}$ is asymptotically stable if all roots of Eq. (10) have negative real parts. The stability analysis is particularly difficult due to the presence of two different exponential functions in the eigenvalue λ. As one parameter is varied a multiple delay differential equation can go through a series of stability switches.

Several authors have investigated the stability regions in a number of special cases. Hale and Huang [24] studied the linear case using as parameters the delays τ_1 and τ_2, while Mahaffy, Joiner, and Zak [26] considered the range $0 < (\tau_1/\tau_2) < 1$ and studied the stability region in a three-dimensional parameter space. Bélair and Campbell [25], Li, Ruan and Wei [28], Shayer and Campbell [29] considered the simpler case in which the left-hand side of the characteristic Eq. (10) is λ instead of $\lambda + 1$. As stated by Bélair and Campbell [25] each of those works has filled in some piece of the puzzle of the two delay stability problem.

The above characteristic Eq. (10) does not have real roots that are positive [simply because the right-hand side of Eq. (10) is negative] so that the stationary state $\tilde{P}$ will become unstable via Hopf bifurcation, thus giving rise to an oscillatory solution. The systems with biological motivation are mainly those with one feedback loop operating quickly (short delay) and another slowly (longer delay). With this consideration in mind, we have set $\tau_1 = 0.26$, $\tau_2 = 2.00$, and we computed the stability region in the parameter space θ_1, n for $\theta_2 \in [0.35, 0.75]$. The boundary at which the Hopf bifurcation occurs corresponds to (θ_1, n) values for which Eq. (10) has a single pair of roots that are pure imaginary, Re $(\lambda) = 0$. In Fig. 1 we display the results when $\theta_2 = 0.491$, and we can see that the stationary state is stable for $n \lesssim 11$. For the range of parameters considered by us, oscil-

latory behavior is observed for n finite greater than 11. The single feedback loop system with parameters $\tau = 2.00, \theta = 0.491$ is stable for $n \leq 2.5$ while the single feedback loop system with parameters $\tau = 0.26, \theta = 0.396$ is stable for $n \leq 11$. Therefore the addition of the quick loop renders the system more stable.

IV. BIFURCATIONS AND CHAOS

In order to demonstrate the existence of chaos in a system with two delays, we shall first look for aperiodic solutions and then check if they result from a period-doubling cascade. We shall consider the cases of finite n (smooth function F), and the $n \to \infty$ limit (piecewise constant function F).

A. Nonlinear equation (finite n)

For fixed values of n, τ_1, and τ_2 Eq. (5) is integrated for each point of the plane (θ_1, θ_2), with θ_1 and θ_2 in the interval $[0.25, 0.75]$. A constant function $[P(t) = 0.4$ for $t \leq 0]$ has been used as an initial function in all the calculations presented below. We used the three-step Gear integrator [31], double precision, using time step of 0.001 for each point of the plane (θ_1, θ_2). Then, for each point (θ_1, θ_2), we consider the time series formed by determining $P(t - 2.00)$ for sucessive crossings of the Poincaré section $P(t) = \tilde{P}$ with $dP/dt < 0$. We shall denote by P_i the value of $P(t - 2.00)$ at the ith crossing of this threshold.

The plot of P_{i+1} vs P_i is called the Poincaré map. The number of points in the Poincaré map indicates the period of the corresponding orbit, i.e., one point corresponds to an orbit with period 1, two points to an orbit with period 2, etc. An infinite number of points indicates the presence of quasiperiodicity or chaotic dynamics. In order to identify those points or regions in the space of parameters (θ_1, θ_2) that may exhibit complex or chaotic dynamics, we discretize the Poincaré section in segments of size 0.001 [32]. For each point on the plane (θ_1, θ_2), we count the number of segments, $K(\theta_1, \theta_2)$, that are visited by the trajectory of the corresponding attractor. The gray scale σ [proportional to $K(\theta_1, \theta_2)$] is used to represent K at a point of the plane (θ_1, θ_2): the maximum (minimum) value of K corresponds to black (white). In Fig. 2 we display the results for $n = 45, \tau_1 = 0.26, \tau_2 = 2.00$. The dark regions correspond to parameter values that may exhibit either complex dynamics or quasiperiodicity. In fact we expect the black regions to correspond to quasiperiodicity as in this case the two-dimensional embedding [33] obtained by plotting $P(t)$ vs $P(t - 2.00)$ will fill the plane more uniformly than in the case of complex dynamics, thus corresponding to larger values of K.

In the dark gray regions in the neighborhood of $\theta_1 = 0.400$, $\theta_2 = 0.500$, and in the neighborhood of $\theta_1 = 0.600$, $\theta_2 = 0.700$, we found both complex dynamics and quasiperiodicity. Figure 3 shows two examples of time delay embedding (left-hand side), and the corresponding Poincaré map (right-hand side). At the top of Fig. 3 we display the case $\theta_1 = 0.396$, $\theta_2 = 0.491$, and at the bottom we display the case $\theta_1 = 0.634$, $\theta_2 = 0.704$. The corresponding Poincaré map
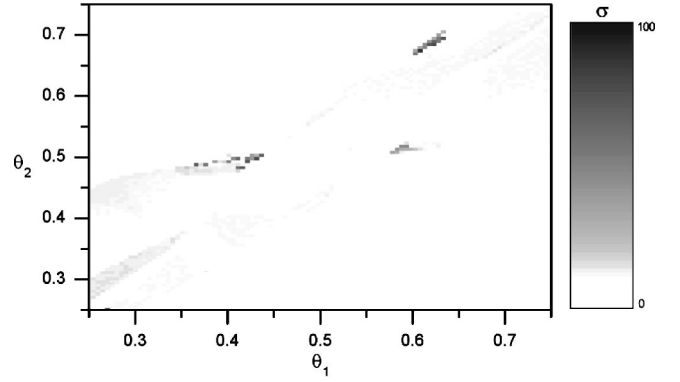
FIG. 2. $K(\theta_1, \theta_2)$ for fixed $\tau_1 = 0.26$, $\tau_2 = 2.00$, $n = 45$ plotted on the plane (θ_1, θ_2) (arbitrary units). We used 100 crossings of the Poincaré section, so $K = 100$ corresponds to σ black. Integration step 0.001.

displayed on the right-hand side of Fig. 3 indicates that the attractor for $\theta_1 = 0.634$, $\theta_2 = 0.704$ is quasiperiodic, while the attractor for $\theta_1 = 0.396$, $\theta_2 = 0.491$ is chaotic. Figure 4 shows the bifurcation diagram of the system (5) on the plane (P, n), with parameters $\theta_1 = 0.396$, $\theta_2 = 0.491$, $\tau_1 = 0.26$, and $\tau_2 = 2.00$. For each value of n the system is first allowed to settle down (the transient is discarded) and then the successive values of P_i are plotted for two hundred iterations. As n increases from 30 through 47, the bifurcation diagram displays a cascade of period-doubling bifurcations and then the inverse cascade that leads to period 3 (that exists for $39 < n < 43$). The attractor for $n = 46$, displayed at the top of Fig. 3, is inside the chaotic region existing beyond the period-3 solution and is followed by another period-doubling cascade. Figure 5 displays the attractor (time delay embedding) and the corresponding Poincaré map for $n = 35$. The Poincaré map has the extremum characteristic of chaotic dynamics [34].

Another way of characterizing a chaotic attractor is by the correlation dimension D_2 and by a positive Lyapunov exponent.

1. Correlation dimension

The correlation dimension D_2 is estimated from the correlation sum [35]

$$C_d(r) = \frac{1}{M_{\text{pairs}}} \sum_{j=1}^{M} \sum_{k=j+w}^{M} \Theta(r - |\mathbf{x}_j - \mathbf{x}_k|), \qquad (11)$$

where $\mathbf{x}_i$ are d-dimensional delay vectors, $M_{\text{pairs}} = (M - d + 1)(M - d - w + 1)/2$ is the number of pairs of points covered by the sums, M is the number of d-dimensional delay vectors, Θ is the Heaviside step function and w will be discussed below. On sufficiently small length scale, and when the embedding dimension d exceeds the dimension of the attractor [36], $C_d(r) \approx r^{D_2}$. Since the attractor dimension is not known *a priori*, one checks for convergence of the estimated values of D_2 with d.

There are many practical problems associated with the computation of the correlation dimension [37,38]. In order to
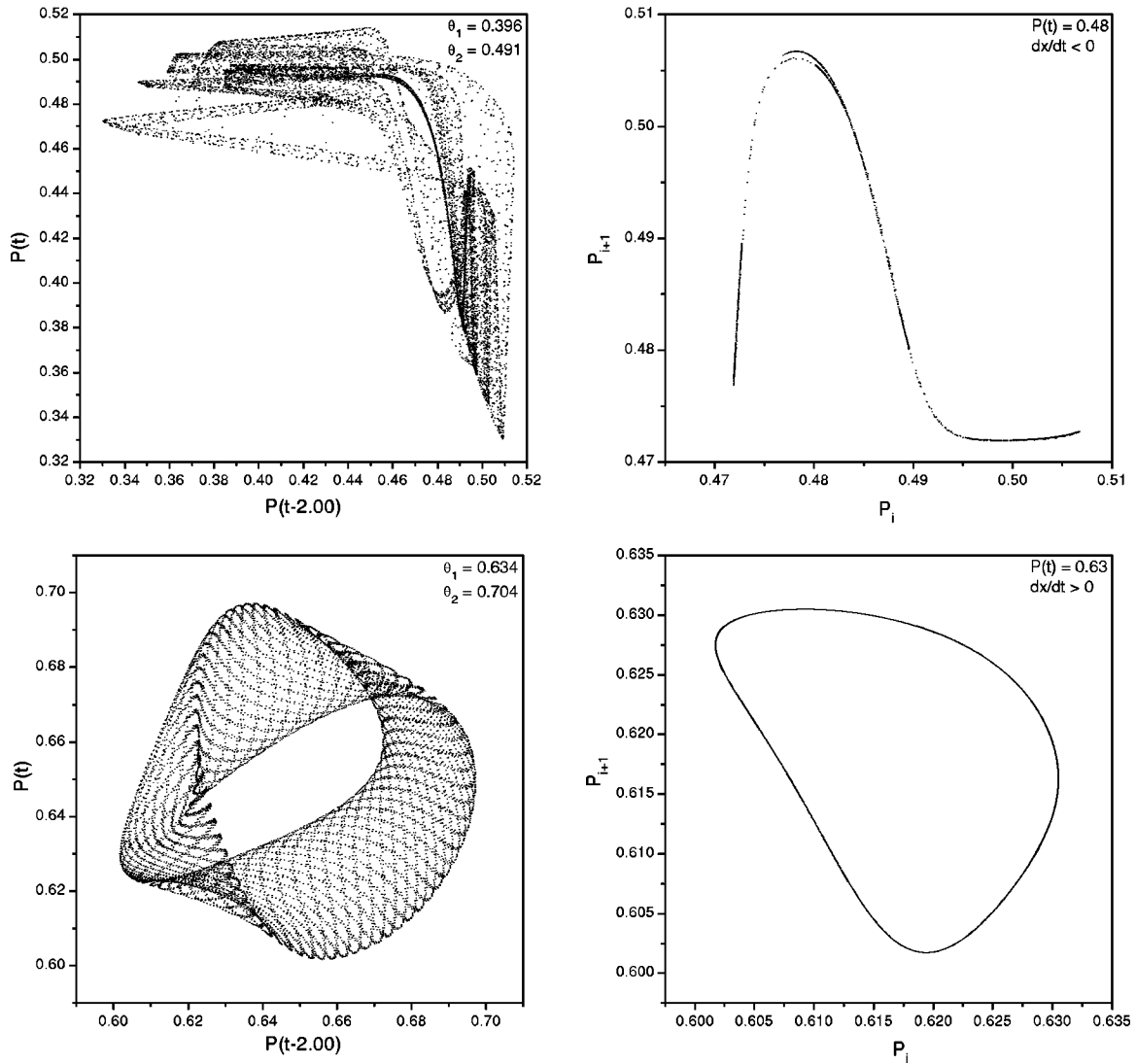
FIG. 3. Phase space $P(t)$ vs $P(t-2.00)$ (on the left), and corresponding Poincaré map (on the right). Parameter values used at the top (bottom): $n=45$, $\theta_1=0.396$, $\theta_2=0.491$ ($n=46$, $\theta_1=0.634$, $\theta_2=0.704$). The same delays were used in both cases: $\tau_1=0.26$, $\tau_2=2.00$. Integration step 0.0001, P is in arbitrary units.

provide a consistent estimate for the correlation integral, the correlation sum should cover a random sample of points drawn independently according to the invariant measure on the attractor. Successive elements of a time series are not usually independent. In particular, for highly sampled flow data, subsequent delay vectors are highly correlated. It is important to exclude temporally correlated points from the pair counting by ignoring all pairs of points in Eq. (11) whose time indices differ by less than w, where w is called the Theiler window w [37]. With $O(M^2)$ pairs available, the loss of $O(M)$ pairs is not dramatic as long as $w \ll M$. At the very least, pairs with $j=k$ ought to be excluded [39]. Otherwise the strong bias towards $D_2=0$ (the mathematically correct value for a finite set of points) will reduce the scaling range drastically.

Parameters in our correlation sum algorithm are, as usual, the embedding dimension d, the time delay τ_2, and the Theiler window that was set to $w=2\tau_2$. All available pairs that satisfy the Theiler criterion contribute to the sum in Eq.
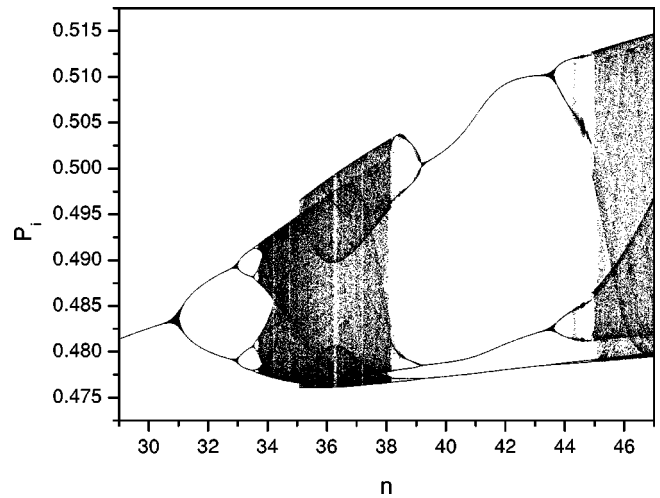
FIG. 4. Bifurcation diagram of Eq. (5) by varying n, with fixed parameters value $\theta_1=0.396$, $\theta_2=0.491$, $\tau_1=0.26$, and $\tau_2=2.00$. Integration step 0.0001, P in arbitrary units, n dimensionless.
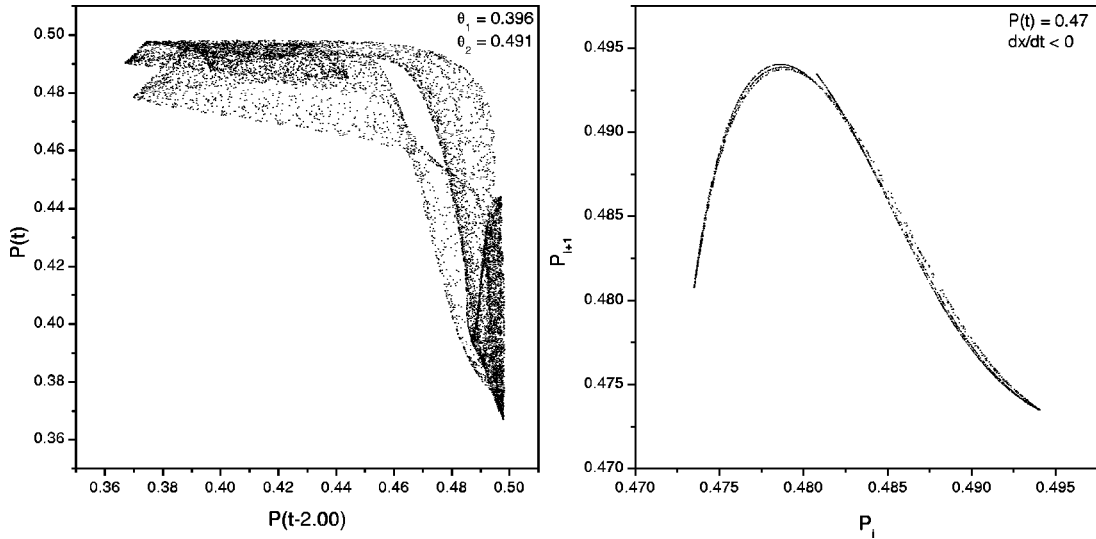
FIG. 5. Phase space $P(t)$ vs $P(t-2.00)$ (on the left), and corresponding Poincaré map (on the right). Parameter values used: $n=35$, $\tau_1=0.26$, $\tau_2=2.00$, and $\theta_1=0.396$, $\theta_2=0.491$. Integration step 0.0001, P in arbitrary units.

(11). The slope of the curve $\log_2 C_d(r)$ vs $\log_2(r)$ is the correlation dimension D_2. In the Fig. 6, we have plotted D_2 vs $\log_2(r)$ of the attractor displayed in the Fig. 5, for several values of the embedding dimension with delay 2.00. With increasing embedding dimension, D_2 converges to a curve with well defined plateau at $D_2 \approx 2.1$ for the attractor shown in the Fig. 5. We also did the calculation for the attractor shown at the top of Fig. 3, and determined $D_2 \approx 1.8$.

2. Maximal Lyapunov exponent

Chaos arises from the exponential growth of infinitesimal perturbations, together with global folding mechanisms to guarantee boundedness of the solutions. This exponential instability is characterized by the spectrum of Lyapunov exponents [40]. If one assumes a local decomposition of the phase space into directions with different stretching or contraction rates, then the spectrum of exponents is the proper average of
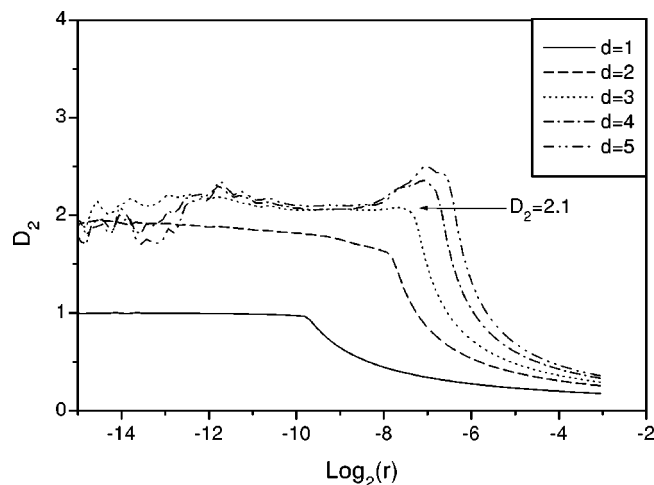
FIG. 6. D_2 of the attractor shown in the Fig. 5. Each curve corresponds to a different embedding dimension d as indicated. Integration step 0.000 02. Both axes are dimensionless.

these local rates over the whole invariant set, and thus consists of as many exponents as there are space directions. The most prominent problem in time series analysis is that the physical phase space is unknown, and that instead the spectrum is computed in some embedding space. Thus the number of exponents depends on the reconstruction, and might be larger than in the physical phase space. Such additional exponents are called spurious, and there are several suggestions to either avoid them [41] or to identify them. Moreover, it is plausible that only as many exponents can be determined from a time series as are entering the Kaplan-Yorke formula. A relevant, and positive, feature of the Lyapunov exponents is that they are invariant under smooth transformations and are thus independent of the measurement function or the embedding procedure. They carry a dimension of inverse time and have to be normalized to the sampling interval.

The maximal Lyapunov exponent can be determined without the explicit construction of a model for the time series. A reliable characterization requires that the independence of embedding parameters and the exponential law for the growth of distances are checked explicitly [42,43].

We implemented the algorithm introduced by Kantz [42] by choosing M reference points $\mathbf{x}_i$ of the time series in the embedding space. Denoting by $U(\mathbf{x}_i, \epsilon)$ the set of reference points $\mathbf{x}_j$ with distance $|\mathbf{x}_j - \mathbf{x}_i| < \epsilon$, we then compute, as a function of l, the average of distances $|\mathbf{x}_{j+l} - \mathbf{x}_{i+l}|$ over all points in $U(\mathbf{x}_i, \epsilon)$. This is done for the M reference points, and we finally compute

$$S(\epsilon,l) = \frac{1}{M} \sum_{i=1}^{M} \ln\left(\frac{1}{|U(\mathbf{x}_i,\epsilon)|} \sum_{\mathbf{x}_j \in U(\mathbf{x}_i,\epsilon)} |\mathbf{x}_{j+l} - \mathbf{x}_{i+l}| \right),$$

(12)

where $|U(\mathbf{x}_i, \epsilon)|$ denotes the cardinality of $U(\mathbf{x}_i, \epsilon)$. If $S(\epsilon,l)$ exhibits a linear increase with identical slope for all embedding dimensions d larger than some d_0, and for a reasonable range of ϵ, then this slope can be taken as an esti-

mate of the maximal Lyapunov exponent [42]. Like other quantities, the maximal Lyapunov exponent estimate may be affected by correlations between reference points and their neighbors. Therefore, a minimum time interval w for $|i-j|$ was considered in the computation (as in the calculation of the correlation dimension D_2).

We have calculated $S(\epsilon,l)$ for the attractors displayed in Figs. 3 and 5, with $0<l<200$ and $\epsilon=2.3\times10^{-4}, 4.6\times10^{-4}, 9.2\times10^{-4}, 18.4\times10^{-4}$. We have observed a clear linear increase of S as function of l, reflecting the exponential divergence of nearby trajectories. The slope is practically the same for $2\leqslant d\leqslant5$ and the maximal Lyapunov exponent equals approximately 0.095 s^{-1} for the attractor in Fig. 5. We have obtained practically the same value for the maximal Lyapunov exponent of the attractor in Fig. 3. We used the Theiler [37] window $w=5\tau_2$. The positive maximal Lyapunov exponents confirm that the attractors in Figs. 3 and 5 are both chaotic.

B. Piecewise linear equation

In the limit when $n_i\rightarrow\infty$, the nonlinear sigmoidal function F in Eq. (3) is a step function, and Eq. (5) is a piecewice linear equation and can be integrated explicitly. Comparing the dynamics obtained by explicit integration of the piecewise linear equation with the dynamics using the numerical methods for n_i large but finite provides a way to check the numerics.

For the parameter values used in Sec. III A, the piecewise linear equation exhibits only periodic solutions. Likewise, the nonlinear Eq. (5) with those parameters value exhibits only periodic solutions for $n>55$. After making a search in the parameter space (using the method described in the beginning of Sec. III A) we selected the parameter values $\tau_1 = 0.65, \theta_1=0.230, \tau_2=2.30, \theta_2=0.217$. Keeping fixed $\theta_1 = 0.230, \theta_2=0.217, \tau_2=2.30$, we constructed the bifurcation diagrams by varying τ_1. The bifurcation diagrams for $\tau_1 \in [0.67, 0.72]$ are displayed in Fig. 7: the result for the piecewise linear equation (step function) is displayed on the left, and for the nonlinear Eq. (5) with $n=400$ is displayed on the right. We selected the value $\tau_1=0.715$ as a possible candidate for complex dynamics, and in Fig. 8 we display the phase plane embedding (at the top), and corresponding Poincaré map (at the bottom), where the piecewise linear case is labeled (a), and the nonlinear case with $n=400$ is labeled (b). Figures 7 and 8 show that the piecewise linear equation (limit $n\rightarrow\infty$) and the nonlinear equation with finite large n exhibit similar dynamics. The Poincaré maps displayed in Fig. 8 are not typical of those found in systems with chaotic dynamics, but are similar to those found in quasiperiodic dynamics. Indeed, the solutions with initial conditions $P(t) = 0.40$ for $t\leqslant0$, and $P(t)=0.39$ for $t\leqslant0$ do not separate exponentially, thus confirming quasiperiodicity. Although for the parameter ranges considered here the piecewise linear equation exhibit only periodic and quasiperiodic solutions, we cannot exclude the possibility of it exhibiting chaotic dynamics for other parameters values.
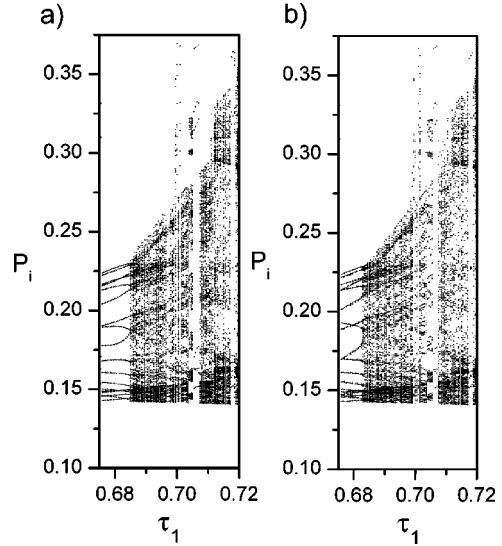
FIG. 7. Bifurcation diagrams varying τ_1: (a) using the step function; (b) using function F (3) with $n=400$ (integration step 0.000 05). Parameters kept fixed: $\tau_2=2.30, \theta_1=0.230, \theta_2=0.217$. P is in arbitray units, and τ_1 is in arbitrary time units.
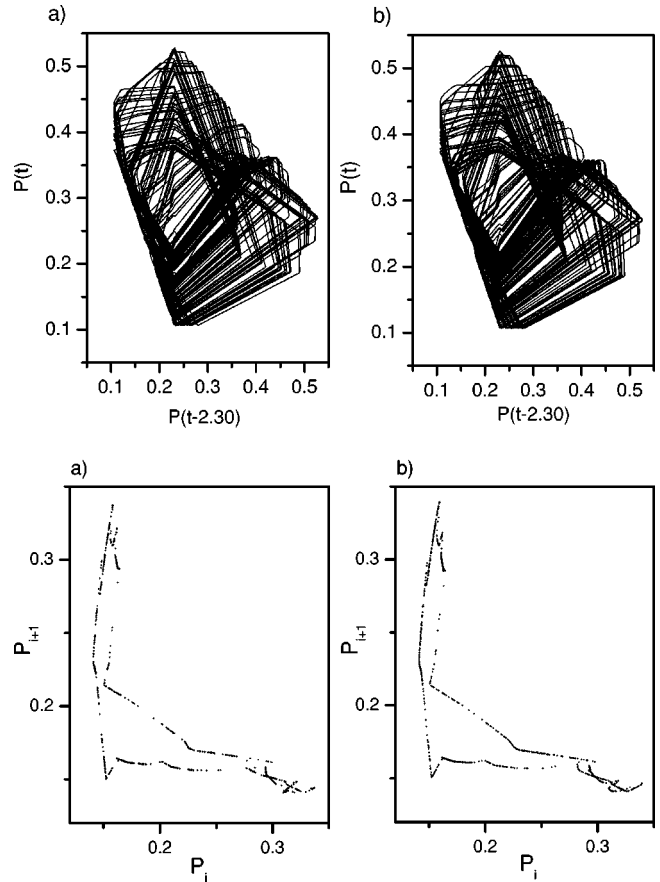
FIG. 8. Phase plane embedding and corresponding Poincaré map for the fixed parameters value $\tau_1=0.715, \tau_2=2.30, \theta_1 = 0.230, \theta_2=0.217$: (a) piecewise linear system ($n\rightarrow\infty$ limit); (b) nonlinear system (4) with $n=400$ (integration step 0.000 001). P in arbitrary units.

V. DISCUSSION AND CONCLUSION

The results presented here show that two-looped delayed negative feedback systems can display low dimensional chaotic dynamics in the case of smooth function F [Eq. (3)]. As the steepness of the delayed feedback is changed by varying n, there is a sequence of period doubling bifurcations as shown in Fig. 4, and chaotic solutions (low dimensional chaotic attractor) found for $n < 50$ as indicated by the positive maximal Lyapunov exponent. For larger values of n, periodic and quasiperiodic dynamics were observed.

Biological systems display complex dynamics and they also contain multiple-delayed feedbacks that play a role in controlling the system dynamics. In most cases, the origin of the complex dynamics is not well known. With the exception of a comparatively small number of cases in which system parameters can be carefully manipulated and controlled, attempts to demonstrate low dimensional chaotic dynamics in biology are rarely convincing. The current work demonstrates the possibility of chaotic dynamics in a system with two delayed negative feedback loops. We have considered the same mathematical model used in [23], for which it was found that in the case with the number of delayed negative feedback loops $N \geq 3$ chaos only exists in a very small range of parameter values. Likewise we find that for $N = 2$, in this class of mathematical model, chaos appears to be a comparatively rare phenomenon. Nevertheless it is important to stress that our mathematical model assumed the variable $P(t)$ to be given by the simple average (2), and we cannot say that chaos is a rare phenomenon if a weighted average is used, the weight also being a parameter that can be varied.

In conclusion, in a situation such that chaos is not a rare phenomenon, it becomes a possible explanation for the fluctuations observed in physiological control systems. Finally, as the equation of the type (5) is used in neural networks [usually in this case the function tanh is used instead of the function (3)] our results might play an important role in designing artificial networks.

[1] U. an der Heiden and M. C. Mackey, J. Math. Biol. **8**, 345 (1982).

[2] M. C. Mackey and L. Glass, Science **197**, 287 (1977).

[3] R. M. May, Ann. N.Y. Acad. Sci. **357**, 267 (1980).

[4] A. I. Mees and P. E. Rapp, J. Math. Biol. **5**, 99 (1978).

[5] L. Glass and M. C. Mackey, *From Clocks to Chaos: The Rhythms of Life* (Princeton University Press, Princeton, NJ, 1988).

[6] H. T. Milhorn, *The Application of Control Theory to Physiological Systems* (Saunders, Philadelphia, PA, 1966).

[7] K. Pakdaman and C. P. Malta, IEEE Trans. Neural Netw. **9**, 231 (1998).

[8] C. P. Malta and C. Grotta-Ragazzo, Int. J. Bifurcation Chaos Appl. Sci. Eng. **1**, 657 (1991).

[9] J. F. Perez, C. P. Malta, and F. A. B. Coutinho, J. Theor. Biol. **71**, 505 (1978).

[10] K. Ikeda, K. Kondo, and O. Akimoto, Phys. Rev. Lett. **49**, 1467 (1982); K. Ikeda and K. Matsumoto, Physica D **29**, 223 (1987).

[11] M. W. Derstine, H. M. Gibbs, F. A. Hopf, and D. L. Kaplan, Phys. Rev. A **27**, 3200 (1983).

[12] C. R. de Oliveira and C. P. Malta, Phys. Rev. A **36**, 3997 (1987).

[13] S. Akselrod, D. Gordon, A. Ubel, D. C. Shannon, A. C. Barger, and R. J. Cohen, Science **213**, 220 (1981).

[14] R. I. Kitney and O. Rompelman, *The Study of Heart Rate Variability* (Clarendon Press, Oxford, 1980).

[15] M. Kobayashi and T. Musha, IEEE Trans. Biomed. Eng. **29**, 456 (1982).

[16] L. Goodman, IEEE Trans. Biomed. Eng. **11**, 82 (1964).

[17] A. W. Cowley, J. F. Liard, and C. Guyton, Circ. Res. **32**, 564 (1973).

[18] L. Glass, A. Beuter, and D. Larocque, Math. Biosci. **90**, 111 (1988).

[19] P. A. Merton, H. B. Morton, and C. Rashbass, Nature (London) **216**, 583 (1967).

[20] M. N. Oĝustötelli and R. B. Stein, J. Math. Biol. **3**, 87 (1976).

[21] A. Beuter, J. Bélair, and C. Labrie, Bull. Math. Biol. **55**, 525 (1993).

[22] A. Beuter and K. Vasilakos, Chaos **5**, 35 (1995).

[23] L. Glass and C. P. Malta, J. Theor. Biol. **145**, 217 (1990).

[24] J. K. Hale and W. Huang, J. Math. Anal. Appl. **178**, 344 (1993).

[25] J. Bélair and S. A. Campbell, SIAM (Soc. Ind. Appl. Math.) J. Appl. Math. **54**, 1402 (1994).

[26] J. P. Mahaffy, K. M. Joiner, and P. J. Zak, Int. J. Bifurcation Chaos Appl. Sci. Eng. **5**, 779 (1995).

[27] L. Olien and J. Bélair, Physica D **102**, 349 (1997).

[28] X. G. Li, S. G. Ruan, and J. J. Wei, J. Math. Anal. Appl. **236**, 254 (1999).

[29] L. P. Shayer and S. A. Campbell, SIAM (Soc. Ind. Appl. Math.) J. Appl. Math. **61**, 673 (2000).

[30] K. Gopalsamy and I. K. C. Leung, IEEE Trans. Neural Netw. **8**, 341 (1997).

[31] In general, this method is more efficient than the Runge-Kutta one because the convergence is achieved for a step that is greater or equal to the step required by the method of Runge-Kutta. See C. P. Malta and M. L. S. Teles, Int. J. Appl. Math. **3**, 379 (2000).

[32] J. C. Bastos de Figueiredo, Ph.D. thesis, IFUSP, 2000.

[33] F. Takens, Lect. Notes Math. **898**, 266 (1986).

[34] M. J. Feigenbaum, J. Stat. Phys. **19**, 25 (1978).

[35] P. Grassberger and I. Procaccia, Physica D **9**, 189 (1983); Phys. Rev. Lett. **50**, 346 (1983).

[36] T. Sauer, J. Yorke, and M. Casdagli, J. Stat. Phys. **65**, 579 (1991).

[37] J. Theiler, Phys. Rev. A **34**, 2427 (1986).

[38] H. Kantz and T. Schreiber, Chaos **5**, 143 (1995).

[39] P. Grassberger, Phys. Lett. A **128**, 369 (1988).

[40] P. Eckmann and D. Ruelle, Rev. Mod. Phys. **57**, 617 (1985).

[41] R. Stoop and J. Parisi, Physica D **50**, 89 (1991).

[42] H. Kantz, Phys. Lett. A **185**, 77 (1994).

[43] M. T. Rosenstein, J. J. Collins, and C. J. De Luca, Physica D **65**, 117 (1993).